

Emergence of New van Hove Singularities in the Charge Density Wave State of a Topological Kagome Metal RbV_3Sb_5

Soohyun Cho,¹ Haiyang Ma^{2,3}, Wei Xia,^{2,4} Yichen Yang,¹ Zhengtai Liu¹, Zhe Huang,¹ Zhicheng Jiang,¹ Xianglu Lu,^{1,5} Jishan Liu,^{1,5} Zhonghao Liu,^{1,5} Jun Li,^{2,4} Jinghui Wang,^{2,4} Yi Liu,⁶ Jinfeng Jia³, Yanfeng Guo,^{2,*} Jianpeng Liu,^{2,4,†} and Dawei Shen^{1,5,‡}

¹Center for Excellence in Superconducting Electronics, State Key Laboratory of Functional Materials for Informatics, Shanghai Institute of Microsystem and Information Technology, Chinese Academy of Sciences, Shanghai 200050, China

²School of Physical Science and Technology, ShanghaiTech University, Shanghai 201210, China

³Key Laboratory of Artificial Structures and Quantum Control (Ministry of Education), Shenyang National Laboratory for Materials Science, School of Physics and Astronomy, Shanghai Jiao Tong University, Shanghai 200240, China

⁴ShanghaiTech Laboratory for Topological Physics, ShanghaiTech University, Shanghai 201210, China

⁵Center of Materials Science and Optoelectronics Engineering, University of Chinese Academy of Sciences, Beijing 100049, China

⁶National Synchrotron Radiation Laboratory, University of Science and Technology of China, Hefei, Anhui 230029, China



(Received 19 May 2021; revised 30 October 2021; accepted 2 November 2021; published 1 December 2021)

Quantum materials with layered kagome structures have drawn considerable attention due to their unique lattice geometry, which gives rise to flat bands together with Dirac-like dispersions. Recently, vanadium-based materials with layered kagome structures were discovered to be topological metals, which exhibit charge density wave (CDW) properties, significant anomalous Hall effect, and unusual superconductivity at low temperatures. Here, we employ angle-resolved photoemission spectroscopy to investigate the electronic structure evolution upon the CDW transition in a vanadium-based kagome material RbV_3Sb_5 . The CDW phase transition gives rise to a partial energy gap opening at the boundary of the Brillouin zone and, most importantly, the emergence of new van Hove singularities associated with large density of states, which are absent in the normal phase and might be related to the superconductivity observed at lower temperatures. Our work sheds light on the microscopic mechanisms for the formation of the CDW and superconducting states in these topological kagome metals.

DOI: [10.1103/PhysRevLett.127.236401](https://doi.org/10.1103/PhysRevLett.127.236401)

A kagome lattice, which is composed of a two-dimensional network of corner-sharing triangles, provides a unique playground for electron correlations and nontrivial band topology. For example, spin systems with antiferromagnetic intersite coupling on kagome lattices are proposed as promising candidates for realizing quantum spin-liquid states [1–6]. Besides, kagome metals usually host electronic structures with coexisting dispersionless flat bands, Dirac cones, and van Hove singularities (VHSs) due to the unique crystal structure, which results in topologically nontrivial states [7–17].

Depending on an electron's filling number, a variety of novel quantum states have been theoretically proposed in kagome lattices, including charge fractionalization [18,19], density wave orders [20–23], topological Chern insulators [24], and superconductivity [22,25]. Particularly, when the band filling of a kagome metal is near the VHS, calculations show that several saddle points would emerge near the Fermi level (E_F) [12,13,22,26]. Coulomb scatterings of electrons between these saddle points would give rise to novel Fermi surface instabilities, which may lead to spin or charge density wave (CDW) states [27–29].

Recently, a new family of AV_3Sb_5 ($A = \text{K}, \text{Rb}, \text{Cs}$) with layered kagome lattices has been discovered [11,12,14,15,30–39]. Previous first principles calculations suggested that bands near the Fermi surfaces in this family of materials are topologically nontrivial and characterized by odd \mathbb{Z}_2 indices [31,32]. Moreover, these vanadium-based kagome metals undergo CDW phase transitions with the critical temperatures $T_{\text{CDW}} \approx 78\text{--}103$ K, below which a new 2×2 inverse star-of-David (ISD) superlattice structure becomes energetically favored [34,36,40,41], leading to a reduction of density of states near E_F [15,34,35,41]. The previous study [36] tried to study the origin of the CDW mechanism with angle-resolved photoemission spectroscopy (ARPES) and scattering measurement, but a consensus on the origin has not been reached. Also, superconductivity emerges from CDW states in these materials if the temperature is further decreased [32]. Surprisingly, a remarkable anomalous Hall effect was observed in the CDW states of these systems [11,42], though so far no clear evidence of long-range magnetic order has been reported. Despite some early attempts [12,13,36,40,43–46], the microscopic mechanisms behind

these intriguing phenomena, such as the driving force for the CDW states, the pairing mechanism and symmetry of the superconducting states, and the origin of the anomalous Hall effect, are still open questions.

In this Letter, combining ARPES and first principles calculations, we study the electronic structure and the microscopic mechanism for the CDW state in RbV_3Sb_5 , which exhibits the highest CDW transition temperature among the AV_3Sb_5 ($A = \text{K}, \text{Rb}, \text{Cs}$) materials [30,32,33]. For the first time, we have observed strong band renormalization effects at low temperatures $T < T_{\text{CDW}}$. We observe a partial energy gap opening at E_F and a shift in the band dispersion to higher binding energy around saddle points. More interestingly, new VHSs around the M points emerge in the CDW phase, which were completely absent in the normal phase. The new VHSs contribute to the large density of states near E_F , which may be related to superconductivity observed at lower temperatures. Moreover, by measuring the zero-frequency joint density of states at the Fermi surface, we find significant charge fluctuations at wave vectors connecting two neighboring M points. We further calculate the phonon dispersions in the normal phase and find unstable modes at both the M and L points. These findings imply that both charge fluctuations at E_F and phonon instabilities in the pristine structure are crucial in driving the system into the CDW phase.

Details of our experiments and calculations can be found in the Supplemental Material [47]. RbV_3Sb_5 crystallizes in a layered hexagonal lattice structure with space group $P6/mmm$ (No. 191). As shown in Fig. 1(a), the system consists of vanadium atoms forming layers of kagome lattices, which are intercalated by Sb atoms forming honeycomb lattice. The vanadium kagome planes are separated by layers of alkali Rb ions forming triangular networks. The in-plane hexagonal lattice constant a is 5.472 \AA , and the out-of-plane lattice constant c is 9.073 \AA . In Fig. 1(a), we show the temperature dependence of the in-plane resistivity for RbV_3Sb_5 , which exhibits an anomaly around 101 K. This anomaly in resistivity is consistent with previous reports [32,33] and is believed to be a hallmark of the CDW phase transition (see the Supplemental Material [47] for details about the sample characteristics and superconducting transition).

We first focus on the normal phase of RbV_3Sb_5 ($T > T_{\text{CDW}}$). According to the photon energy dependent ARPES measurements, a weak k_z dispersion is observed, consistent with a quasi-2D band structure along the k_z direction (see the Supplemental Material [47] for the discussion about k_z dependent measurements). Figure 1(e) illustrates the photoemission intensity map in the k_x - k_y plane measured at 200 K with 19 eV photons, which corresponds to Fermi surface of RbV_3Sb_5 on the $\bar{\Gamma}$ - \bar{M} - \bar{K} plane. Besides, in Fig. 1(c) we show the photoemission intensity plot along the high-symmetry path connecting $\bar{\Gamma}$ - \bar{K} - \bar{M} - $\bar{\Gamma}$ points. Combining Figs. 1(c) and 1(e), it can be clearly seen that the

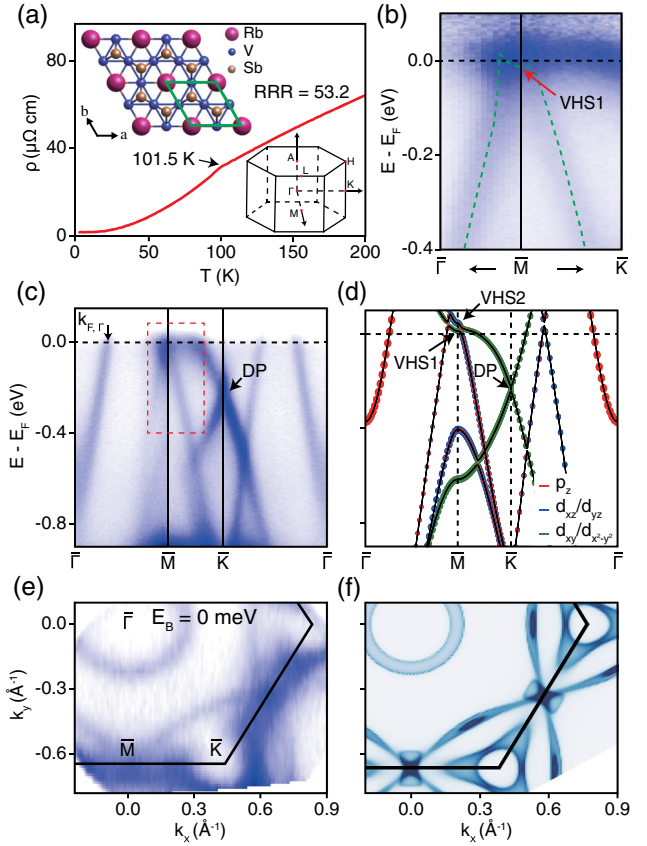


FIG. 1. (a) The resistivity versus temperature curve with the anomaly near the 101 K, signifying the charge density wave phase transition. The upper left corner inset is the top view of crystal structure of RbV_3Sb_5 , and the bottom right corner inset is a three-dimensional hexagonal BZ with high symmetry point. (b) Enlarged plot of the band dispersion in the red box on (c). The ARPES spectra are divided by the Fermi-Dirac distribution function to visualize the band dispersion above E_F . The green dotted line is a guide for the eye. (c) The ARPES spectra above T_{CDW} along the $\bar{\Gamma}$ - \bar{M} - \bar{K} - $\bar{\Gamma}$ direction and (d) the calculated band structure including spin-orbit coupling along the same high-symmetry path as (c). (e) Experimentally obtained Fermi surface map at 19 eV and above T_{CDW} . (f) The energy constant map taken from the band calculations corresponding to the Fermi level of ARPES data. The back line indicates the hexagonal BZ of the kagome lattice.

system possesses an electron pocket around $\bar{\Gamma}$, a Dirac-cone-like dispersion around \bar{K} point, and some relatively flat dispersions with large intensity near the \bar{M} point.

In Figs. 1(d) and 1(f), we demonstrate the calculated band structure along the $\bar{\Gamma}$ - \bar{K} - \bar{M} - $\bar{\Gamma}$ path and calculated Fermi surface map on the $\bar{\Gamma}$ - \bar{M} - \bar{K} plane, respectively, both of which are in good agreement with experiments. Neglecting spin-orbit coupling (SOC), calculations show that the Dirac point at the \bar{K} point is fourfold degenerate (including spin degeneracy), which is protected by C_{3z} , inversion, and time-reversal symmetries of RbV_3Sb_5 in its normal state. Similar Dirac points in the absence of SOC

have been observed in other transition-metal based kagome lattices [7,8,16]. Including SOC would open a gap ~ 20 meV at the Dirac point, which is indeed observed in our ARPES measurement (see the Supplemental Material [47] for the detail). The calculations further indicate that the Dirac cone near the K point consists mostly of vanadium d_{xy} and $d_{x^2-y^2}$ orbitals, while the electron pocket around Γ is contributed to mainly by the antimony p_z orbitals. Moreover, we found that two VHSs near the M point are located slightly below and above the E_F [marked as VHS1 and VHS2 in Fig. 1(d)], respectively. In both ARPES measurements and density functional theory calculations, VHS1 exhibits upward dispersion along the $\bar{M}-\bar{\Gamma}$ path and downward dispersion along the $\bar{M}-\bar{K}$ path, as shown in Figs. 1(b) and 1(d). These lead to large density of states around the \bar{M} points near E_F , which may introduce Fermi surface instabilities at wave vectors connecting two \bar{M} points.

We then turn to discuss the electronic structure in the CDW phase of RbV_3Sb_5 . When $T < T_{\text{CDW}}$, the system forms a 2×2 ISD type superstructure as shown in Fig. 2(a) [34,40,41], and our first principles calculations indicate that such a structure is energetically favored. It is worthy to note that recent studies suggest there is additional cell doubling or even quadrupling along the c axis [15,44,58]. However, since the states around the VHSs near the M points and the Dirac point are of in-plane orbital characters [Fig. 1(d)], the

cell doubling or quadrupling along the c axis does not significantly change the electronic structure around the M point and the Dirac point; thus, in this work we only consider the in-plane 2×2 ISD structure in the calculations. The BZ of the ISD supercell is one quarter of the pristine BZ [Fig. 2(b)]; therefore, the energy bands from the pristine lattice would be folded from the original BZ to the ISD supercell BZ, which may open up gaps at the supercell BZ boundary. However, experimentally we hardly discover any spectral weight of the folded bands, as shown in Fig. 2(c), suggesting a weak charge-modulation effect in the CDW phase of RbV_3Sb_5 with ISD structure.

Although the band-folding effect is weak, we indeed find that the CDW transition would result in an orbital-selective variation of the band structure compared to that of the normal phase. First, as shown in Fig. 2(c), the Fermi wave vector k_F of the electron pocket around $\bar{\Gamma}$ increases from 0.257 \AA^{-1} in the normal state to 0.262 \AA^{-1} with a dramatic sinking of this band due to the CDW transition. As the electron pocket around Γ is mostly contributed to by the out-of-plane p_z orbitals, a strong energy shift at $\bar{\Gamma}$ implies a possible cell doubling or quadrupling along the c axis. In sharp contrast, the Dirac band around the \bar{K} point, mainly of a in-plane orbital character, remains nearly intact upon the phase transition. Such behavior is reminiscent of that in bulk $1T\text{-TiSe}_2$, which is well known as a $2 \times 2 \times 2$ CDW

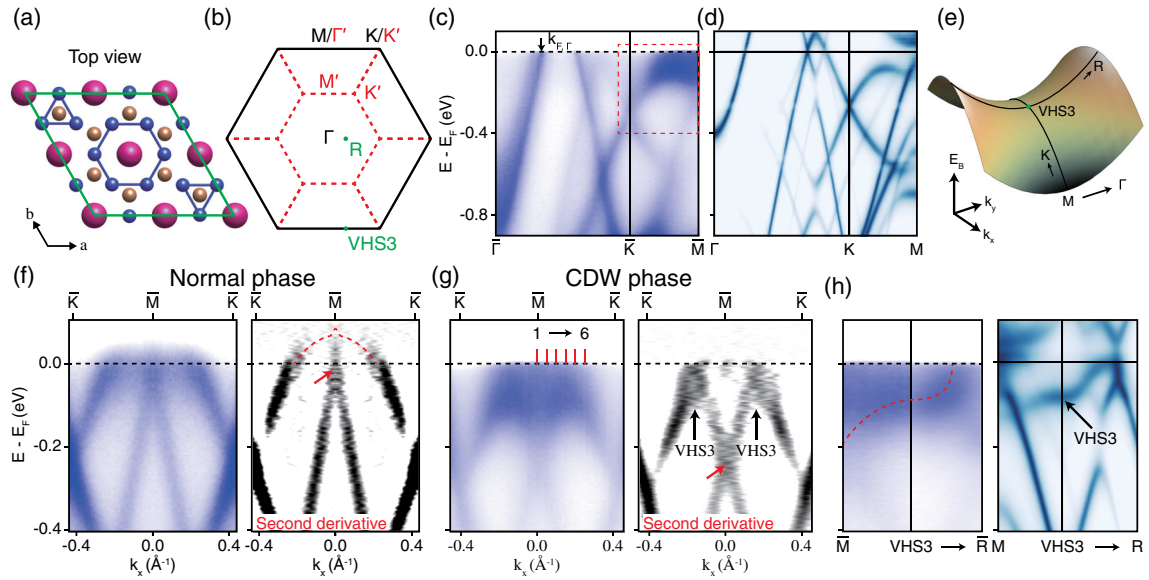


FIG. 2. (a) The image of vanadium-based kagome lattice under the 2×2 charge density wave, which is consistent with the ISD superlattice. The green line indicates the unit cell of 2×2 superstructure of ISD. (b) The hexagonal BZ (black line) and the folded BZ of 2×2 superstructure (red dotted line). (c) ARPES spectra of CDW phase along the $\bar{\Gamma}-\bar{K}-\bar{M}$ direction taken with 55 eV photon energy at 10 K, below T_{CDW} , and (d) the calculated spectral function for the ISD CDW phase unfolded to the pristine BZ. (e) Schematic picture of the saddle point near the VHS3. The high symmetry cut along the \bar{M} to \bar{K} direction obtained from the normal phase ($> T_{\text{CDW}}$) (f) and the CDW phase ($< T_{\text{CDW}}$) (g). The second derivative spectra of the left panel to enhanced the visibility of the band near the \bar{M} point. (h) The ARPES spectra and the calculated unfolded spectra of $2 \times 2 \times 1$ ISD along the M -VHS3- R direction. The red dotted line is a guide for the eye.

material [59]. This finding implies the possible charge modulation along the c axis in RbV_3Sb_5 , as also suggested by some previous reports [15,58].

Besides, the CDW phase transition gives rise to significant change of spectra around the \bar{M} point, as shown by the direct comparison of the photoemission intensity plots measured in the normal and CDW states [Figs. 2(f) and 2(g)]. Evidently, nearly the whole VHS1 in the normal state is pushed downward in binding energy, while only a small region of the higher VHS2 close to the \bar{M} point is gapped, resulting in the “M”-shaped band dispersion along the \bar{K} - \bar{M} - \bar{K} path in Fig. 2(g). Here, second derivative spectra are provided as well in order to enhance the visibility of the CDW-induced spectral weight shift around the \bar{M} point. Comparing the energy positions of the VHS1 saddle point in the normal phase and in the CDW phase [indicated by the red arrows in Figs. 2(f) and 2(g)], we estimate an energy shift of about 200 meV induced by the CDW transition. More interestingly, a new VHS (marked as VHS3 thereafter) emerges in the CDW phase, and its saddle point is located somewhere close to \bar{M} , as illustrated in Figs. 2(g) and 2(h) and Fig. S3 in the Supplemental Material [47]. This finding is supported by calculations based on a $2 \times 2 \times 1$ ISD structure [Fig. 2(d) and the right panel of Fig. 2(h)] as well as is in good agreement with another measurement [12,34]. The large density of states (DOS) introduced by this emergent VHS3 in RbV_3Sb_5 may be intimately relevant to superconductivity due to enhanced electron-phonon coupling near the Fermi surface [60–63].

Figures 3(b)–3(g) show the detailed temperature dependent evolution of VHSs around \bar{M} across T_{CDW} . When the temperature is above T_{CDW} , as schematically illustrated in Fig. 3(a), both VHS1 and VHS2 around the \bar{M} point are in the vicinity of E_F , and they almost remain intact with decreasing temperature, as shown in Figs. 3(b) and 3(c). However, once the temperature is below T_{CDW} , states around the \bar{M} point are gradually shifted to higher binding energy, eventually leading to a large downshift ~ 200 meV for states at \bar{M} , and an “M”-shaped band dispersion appears at 10 K [Fig. 3(h)]. Such temperature dependence of the gapped spectral weight around \bar{M} has unambiguously illustrated its CDW origin. Moreover, we also present the photoemission energy distribution curves (EDCs) taken around \bar{M} in Fig. 3(i). We found that one more shoulderlike peak (marked by red triangles) in the EDC suddenly emerges below T_{CDW} and is continuously pushed to higher binding energy with the decrease of temperature, which demonstrates a complete picture of the CDW gap development in RbV_3Sb_5 .

In order to better understand the microscopic mechanism for the formation of the CDW state, we calculate the zero-frequency joint DOS contributed by the Fermi surface:

$$C(\mathbf{q}) = \frac{\Omega_0}{(2\pi)^3} \int d\mathbf{k} A(\mathbf{k}, E_F) A(\mathbf{k} + \mathbf{q}, E_F), \quad (1)$$

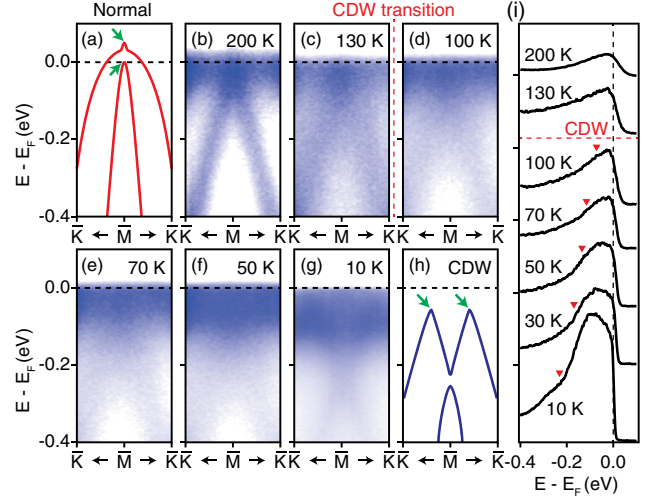


FIG. 3. Temperature-dependent ARPES measurements taken from the 19 and 55 eV near the \bar{M} point. (a) and (h) schematic picture of the band structure of the normal and CDW phase, respectively. (b)–(g) The holelike band at the \bar{M} point is shifted to higher binding energy as the temperature decreases. The green arrows indicate the VHS at the schematic figure. (i) Corresponding EDCs at the \bar{M} point for data in (b)–(g) to reveal the evolution of the peak shift. The red mark indicates the emergence of the peak below the CDW transition temperature.

where $A(\mathbf{k}, E_F)$ is the spectral function at E_F at the \mathbf{k} point in the BZ, and Ω_0 is the volume the primitive cell. $C(\mathbf{q})$ describes the phase space for the scatterings of electrons from the states at \mathbf{k} to those at $\mathbf{k} + \mathbf{q}$ at the Fermi surface, which is a characterization of the Fermi-surface charge fluctuations with wave vector \mathbf{q} . Therefore, it is expected that $C(\mathbf{q})$ would show a peak at the corresponding ordering wave vector if there exists any charge instability induced by charge fluctuations at the Fermi surface. This autocorrelation of ARPES spectra in the normal state has been demonstrated to give a reasonable count for charge-ordering instabilities of various compounds [64–67]. The $C(\mathbf{q})$ map extracted from ARPES spectra is shown in Fig. 4(a), which exhibits several peaks at wave vectors \mathbf{q}_i ($i = 1, 2$ and 3) (see the Supplemental Material [47] for detail). This is consistent with the calculated zero-frequency joint DOS shown in Fig. 4(b). We find that $\{\mathbf{q}_i\}$ are rather close to “nesting” wave vectors connecting the different saddle points (around M) at the Fermi surface in the BZ, as schematically shown in Fig. 4(c). This indicates that the strong charge fluctuations due to the Fermi-surface nesting are an important driving force for the formation of the CDW state in RbV_3Sb_5 .

Moreover, we have also calculated the phonon dispersion along the high-symmetry path as shown in Fig. 4(d), which clearly shows two unstable modes around the M and L points, respectively. The soft phonon mode at the M point and the strong charge fluctuations at \mathbf{q}_1 would cooperate with each other, both of which tend to drive the

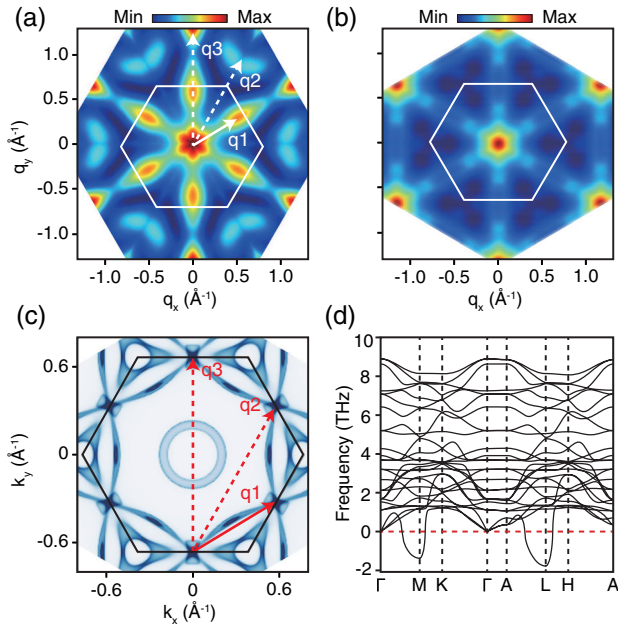


FIG. 4. (a) Two-dimensional joint DOS results on the saddle band point regions. (b) Calculated joint DOS at the Fermi energy. (c) Calculated Fermi surface projected to the k_x - k_y plane. (d) Calculated phonon spectrum along a high-symmetry path. The high-symmetry points are marked in Fig. 1(a).

system into a CDW state that doubles the primitive cell along the \mathbf{q}_1 direction in the kagome plane. However, since there are three equivalent \mathbf{q}_1 wave vectors (three equivalent M points) in the BZ, these three \mathbf{q}_1 vectors may be linked with the three sublattices in the kagome lattice, forming a “triple-Q” CDW state preserving C_{3z} symmetry [43], which is exactly the 2×2 ISD structure. The additional soft phonon mode at the L point may be the origin of the cell doubling along the c axis in the CDW phase. Detailed discussions about the soft phonon modes and their effects on electrons’ band energies are given in the Supplemental Material [47].

To summarize, we have studied the electronic structures of a kagome metal RbV_3Sb_5 in the normal and CDW phases. We have revealed partial gap opening at saddle points, orbital-selective band energy shift, and the emergence of new VHSs near E_F induced by the CDW. We uncover that the CDW phase is driven by the Fermi surface nesting of van Hove singularities at neighboring saddle points, which are further assisted by an unstable phonon mode at the same nesting wave vector. Our work is a significant step forward in understanding the mysterious CDW phase in the V-based topological kagome metals.

This work was supported by the National Science Foundation of China (Grants No. U2032208, No. 92065201, and No. 11874264), the National Key R&D Program of the MOST of China (Grant No. 2016YFA0300204), and the Natural Science Foundation of Shanghai (Grant

No. 14ZR1447600). Y. F. G. acknowledges the starting grant of ShanghaiTech University and the Program for Professor of Special Appointment (Shanghai Eastern Scholar). J. S. L. thanks the fund of Science and Technology on Surface Physics and Chemistry Laboratory (6142A02200102). Part of this research used Beamline 03U of the Shanghai Synchrotron Radiation Facility, which is supported by ME² project under Contract No. 11227902 from National Natural Science Foundation of China. J. P. L. acknowledge the support from the National Key R & D program of China (Grant No. 2020YFA0309601), and the start-up grant of ShanghaiTech University. The authors also acknowledge the support from the Analytical Instrumentation Center (#SPST-AIC10112914), SPST, ShanghaiTech University.

S. C., H. M., and W. X., made equal contributions to this work.

*Corresponding author.

guoyf@shanghaitech.edu.cn

†Corresponding author.

liujp@shanghaitech.edu.cn

‡Corresponding author.

dwshen@mail.sim.ac.cn

- [1] D. E. Freedman, T. H. Han, A. Prodi, P. Muller, Q.-Z. Huang, Y.-S. Chen, S. M. Webb, Y. S. Lee, T. M. McQueen, and D. G. Nocera, *J. Am. Chem. Soc.* **132**, 16185 (2010).
- [2] T. Han, S. Chu, and Y. S. Lee, *Phys. Rev. Lett.* **108**, 157202 (2012).
- [3] M.-X. Fu, T. Imai, T.-H. Han, and Y. S. Lee, *Science* **350**, 655 (2015).
- [4] S. Yan, D. A. Huse, and S. R. White, *Science* **332**, 1173 (2011).
- [5] D. Wulferding, P. Lemmens, P. Scheib, J. Röder, P. Mendels, S.-Y. Chu, T.-H. Han, and Y. S. Lee, *Phys. Rev. B* **82**, 144412 (2010).
- [6] T.-H. Han, J. S. Helton, S. Chu, D. G. Nocera, J. A. Rodriguez-Rivera, C. Broholm, and Y. S. Lee, *Nature (London)* **492**, 406 (2012).
- [7] M. Kang *et al.*, *Nat. Mater.* **19**, 163 (2020).
- [8] L. Ye, M. Kang, J.-W. Liu, F. Von Cube, C. R. Wicker, T. Suzuki, C. Jozwiak, A. Bostwick, E. Rotenberg, D. C. Bell, L. Fu, R. Comin, and J. G. Checkelsky, *Nature (London)* **555**, 638 (2018).
- [9] E. Liu *et al.*, *Nat. Phys.* **14**, 1125 (2018).
- [10] D.-F. Liu, A.-J. Liang, E.-K. Liu, Q.-N. Xu, Y.-W. Li, C. Chen, D. Pei, W.-J. Shi, S. K. Mo, P. Dudin, T. Kim, C. Cacho, G. Li, Y. Sun, L.-X. Yang, Z.-K. Liu, S. S. P. Parkin, C. Felser, and Y.-L. Chen, *Science* **365**, 1282 (2019).
- [11] S.-Y. Yang, Y. Wang, B. R. Ortiz, D. Liu, J. Gayles, E. Derunova, R. Gonzalez-Hernandez, L. Šmejkal, Y. Chen, S. S. P. Parkin, S. D. Wilson, E. S. Toberer, T. McQueen, and M. N. Ali, *Sci. Adv.* **6**, eabb6003 (2020).
- [12] X. Zhou, Y. Li, X. Fan, J. Hao, Y. Dai, Z. Wang, Y. Yao, and H.-H. Wen, *Phys. Rev. B* **104**, L041101 (2021).
- [13] X. Wu, T. Schwemmer, T. Müller, A. Consiglio, G. Sangiovanni, D. D. Sante, Y. Iqbal, W. Hanke, A. P.

- Schnyder, M. M. Denner, M. H. Fischer, T. Neupert, and R. Thomale, *Phys. Rev. Lett.* **127**, 177001 (2021).
- [14] Y. Hu, S. M. L. Teicher, B. R. Ortiz, Y. Luo, S. Peng, L. Huai, J. Z. Ma, N. C. Plumb, S. D. Wilson, J.-F. He, and M. Shi, [arXiv:2104.12725](https://arxiv.org/abs/2104.12725).
- [15] Z. Liang, X. Hou, W. Ma, F. Zhang, P. Wu, Z. Zhang, F. Yu, J. J. Ying, K. Jiang, L. Shan, Z. Wang, and X. H. Chen, *Phys. Rev. X* **11**, 031026 (2021).
- [16] Z. Liu, M. Li, Q. Wang, G. Wang, C. Wen, K. Jiang, X. Lu, S. Yan, Y. Huang, D. Shen, J.-X. Yin, Z. Wang, Z. Yin, H. Lei, and S. Wang, *Nat. Commun.* **11**, 4002 (2020).
- [17] M. Li, Q. Wang, G. Wang, Z. Yuan, W. Song, R. Lou, Z. Liu, Y. Huang, Z. Liu, H. Lei, Z. Yin, and S. Wang, *Nat. Commun.* **12**, 3129 (2021).
- [18] A. O'Brien, F. Pollmann, and P. Fulde, *Phys. Rev. B* **81**, 235115 (2010).
- [19] A. Rüegg and G. A. Fiete, *Phys. Rev. B* **83**, 165118 (2011).
- [20] H.-M. Guo and M. Franz, *Phys. Rev. B* **80**, 113102 (2009).
- [21] S. V. Isakov, S. Wessel, R. G. Melko, K. Sengupta, and Y. B. Kim, *Phys. Rev. Lett.* **97**, 147202 (2006).
- [22] W.-S. Wang, Z.-Z. Li, Y.-Y. Xiang, and Q.-H. Wang, *Phys. Rev. B* **87**, 115135 (2013).
- [23] B. R. Ortiz, S. M. L. Teicher, L. Kautzsch, P. M. Sarte, J. P. C. Ruff, R. Seshadri, and S. D. Wilson, *Phys. Rev. X* **11**, 041030 (2021).
- [24] G. Xu, B. Lian, and S.-C. Zhang, *Phys. Rev. Lett.* **115**, 186802 (2015).
- [25] W.-H. Ko, P. A. Lee, and X.-G. Wen, *Phys. Rev. B* **79**, 214502 (2009).
- [26] K. Barros, J. W. F. Venderbos, G.-W. Chern, and C. D. Batista, *Phys. Rev. B* **90**, 245119 (2014).
- [27] M. L. Kiesel and R. Thomale, *Phys. Rev. B* **86**, 121105(R) (2012).
- [28] M. L. Kiesel, C. Platt, and R. Thomale, *Phys. Rev. Lett.* **110**, 126405 (2013).
- [29] C. Nayak, *Phys. Rev. B* **62**, 4880 (2000).
- [30] B. R. Ortiz, L. C. Gomes, J. R. Morey, M. Winiarski, M. Bordelon, J. S. Mangum, I. W. H. Oswald, J. A. Rodriguez-Rivera, J. R. Neilson, S. D. Wilson, E. Ertekin, T. M. McQueen, and E. S. Toberer, *Phys. Rev. Mater.* **3**, 094407 (2019).
- [31] B. R. Ortiz, P. M. Sarte, E. M. Kenney, M. J. Graf, S. M. L. Teicher, R. Seshadri, and S. D. Wilson, *Phys. Rev. Mater.* **5**, 034801 (2021).
- [32] B. R. Ortiz, S. M. L. Teicher, Y. Hu, J. L. Zuo, P. M. Sarte, E. C. Schueller, A. M. M. Abeykoon, M. J. Krogstad, S. Rosenkranz, R. Osborn, R. Seshadri, L. Balents, J. He, and S. D. Wilson, *Phys. Rev. Lett.* **125**, 247002 (2020).
- [33] Q. Yin, Z. Tu, C. Gong, Y. Fu, S. Yan, and H. Lei, *Chin. Phys. Lett.* **38**, 037403 (2021).
- [34] Y.-X. Jiang *et al.*, *Nat. Mater.* **20**, 1353 (2021).
- [35] H. Chen *et al.*, *Nature (London)* **599**, 222 (2021).
- [36] H.-X. Li, T.-T. Zhang, Y.-Y. Pai, C. Marvinney, A. Said, T. Yilmaz, Q. Yin, C. Gong, Z. Tu, E. Vescovo, R. Moore, S. Murakami, H.-C. Lei, H. Lee, B. Lawrie, and H. Miao, *Phys. Rev. X* **11**, 031050 (2021).
- [37] Z.-H. Liu, N.-N. Zhao, Q.-W. Yin, C.-S. Gong, Z.-J. Tu, M. Li, W.-H. Song, Z.-T. Liu, D.-W. Shen, Y.-B. Huang, K. Liu, H.-C. Lei, and S.-C. Wang, *Phys. Rev. X* **11**, 041010 (2021).
- [38] K. Nakayama, Y. Li, M. Liu, Z. Wang, T. Takahashi, Y. Yao, and T. Sato, *Phys. Rev. B* **104**, L161112 (2021).
- [39] Z. Wang, S. Ma, Y. Zhang, H. Yang, Z. Zhao, Y. Ou, Y. Zhu, S. Ni, Z. Lu, H. Chen, K. Jiang, L. Yu, Y. Zhang, X. Dong, J. Hu, H.-J. Gao, and Z. Zhao, [arXiv:2104.05556](https://arxiv.org/abs/2104.05556).
- [40] N. Ratcli, L. Hallett, B. R. Ortiz, S. D. Wilson, and J. W. Harter, [arXiv:2104.10138](https://arxiv.org/abs/2104.10138).
- [41] H.-X. Tan, Y.-Z. Liu, Z.-Q. Wang, and B.-H. Yan, *Phys. Rev. Lett.* **127**, 046401 (2021).
- [42] F.-H. Yu, T. Wu, Z.-Y. Wang, B. Lei, W.-Z. Zhuo, J.-J. Ying, and X.-H. Chen, *Phys. Rev. B* **104**, L041103 (2021).
- [43] X.-L. Feng, K. Jiang, Z.-Q. Wang, and J.-P. Hu, *Sci. Bull.* **66**, 1384 (2021).
- [44] T. Park, M.-X. Ye, and L. Balents, *Phys. Rev. B* **104**, 035142 (2021).
- [45] Y.-P. Lin and R. M. Nandkishore, *Phys. Rev. B* **104**, 045122 (2021).
- [46] M. M. Denner, R. Thomale, and T. Neupert, [arXiv:2103.14045](https://arxiv.org/abs/2103.14045).
- [47] See Supplemental Material, which includes Refs. [30,33, 48–57], at <http://link.aps.org/supplemental/10.1103/PhysRevLett.127.236401> for details of single crystal synthesis, characterization, ARPES measurements and calculations.
- [48] Y.-C. Yang, Z.-T. Liu, J.-S. Liu, Z.-H. Liu, W.-L. Liu, X.-L. Lu, H.-P. Mei, A. Li, M. Ye, S. Qiao, and D.-W. Shen, *Nucl. Sci. Tech.* **32**, 31 (2021).
- [49] G. Kresse and J. Furthmüller, *Comput. Mater. Sci.* **6**, 15 (1996).
- [50] J. P. Perdew, K. Burke, and M. Ernzerhof, *Phys. Rev. Lett.* **77**, 3865 (1996).
- [51] P. E. Blöchl, *Phys. Rev. B* **50**, 17953 (1994).
- [52] G. Kresse and D. Joubert, *Phys. Rev. B* **59**, 1758 (1999).
- [53] A. Togo and I. Tanaka, *Scr. Mater.* **108**, 1 (2015).
- [54] A. A. Mostofi, J. R. Yates, Y.-S. Lee, I. Souza, D. Vanderbilt, and N. Marzari, *Comput. Phys. Commun.* **178**, 685 (2008).
- [55] Y. Hu, X. Wu, B. R. Ortiz, S. Ju, X. Han, J. Z. Ma, N. C. Plumb, M. Radovic, R. Thomale, S. D. Wilson, A. P. Schnyder, and M. Shi, [arXiv:2106.05922](https://arxiv.org/abs/2106.05922).
- [56] M. Kang, S. Fang, J.-K. Kim, B. R. Ortiz, J. Yoo, B.-G. Park, S. D. Wilson, J.-H. Park, and R. Comin, [arXiv:2105.01689](https://arxiv.org/abs/2105.01689).
- [57] S. Y. Zhou, G.-H. Gweon, A. V. Fedorov, P. N. First, W. A. De Heer, D.-H. LEE, F. Guinea, A. H. Castro Neto, and A. Lanzara, *Nat. Mater.* **6**, 770 (2007).
- [58] E. Uykur, B. R. Ortiz, S. D. Wilson, M. Dressel, and A. A. Tsirlin, [arXiv:2103.07912](https://arxiv.org/abs/2103.07912).
- [59] A. Wegner, J. Zhao, J. Li, J. Yang, A. A. Anikin, G. Karapetrov, K. Esfarjani, D. Louca, and U. Chatterjee, *Phys. Rev. B* **101**, 195145 (2020).
- [60] C. Mielke, III, Y. Qin, J.-X. Yin, H. Nakamura, D. Das, K. Guo, R. Khasanov, J. Chang, Z. Q. Wang, S. Jia, S. Nakatsuji, A. Amato, H. Luetkens, G. Xu, M. Z. Hasan, and Z. Guguchia, *Phys. Rev. Mater.* **5**, 034803 (2021).
- [61] K. Kim, S. Kim, J. S. Kim, H. Kim, J.-H. Park, and B. I. Min, *Phys. Rev. B* **97**, 165102 (2018).
- [62] D. M. Newns, H. R. Krishnamurthy, P. C. Pattnaik, C. C. Tsuei, and C. L. Kane, *Phys. Rev. Lett.* **69**, 1264 (1992).
- [63] K. Gofron, J. C. Campuzano, A. A. Abrikosov, M. Lindroos, A. Bansil, H. Ding, D. Koelling, and B. Dabrowski, *Phys. Rev. Lett.* **73**, 3302 (1994).

- [64] D.-W. Shen, B.-P. Xie, J.-F. Zhao, L.-X. Yang, L. Fang, J. Shi, R.-H. He, D.-H. Lu, H.-H. Wen, and D.-L. Feng, *Phys. Rev. Lett.* **99**, 216404 (2007).
- [65] U. Chatterjee, M. Shi, A. Kaminski, A. Kanigel, H. M. Fretwell, K. Terashima, T. Takahashi, S. Rosenkranz, Z. Z. Li, H. Raffy, A. Santander-Syro, K. Kadowaki, M. R. Norman, M. Randeria, and J. C. Campuzano, *Phys. Rev. Lett.* **96**, 107006 (2006).
- [66] K. McElroy, G.-H. Gweon, S.-Y. Zhou, J. Graf, S. Uchida, H. Eisaki, H. Takagi, T. Sasagawa, D.-H. Lee, and A. Lanzara, *Phys. Rev. Lett.* **96**, 067005 (2006).
- [67] D.-W. Shen, Y. Zhang, L.-X. Yang, J. Wei, H.-W. Ou, J.-K. Dong, B.-P. Xie, C. He, J.-F. Zhao, B. Zhou, M. Arita, K. Shimada, H. Namatame, M. Taniguchi, J. Shi, and D.-L. Feng, *Phys. Rev. Lett.* **101**, 226406 (2008).